JOURNAL OF AERONAUTICS AND SPACE TECHNOLOGIES
(ISSN : 1304-0448)
January 2021 Volume 14 Number 1
www.jast.hho.edu.tr

Research Article

An Open-Source Hypersonic Solver For Non-equilibrium Flows

Davut VATANSEVER[1], Bayram ÇELİK[2]

[1] *Istanbul Technical University, Department of Astronautical Engineering, 34469 Sariyer , Istanbul, Turkey*, vatansever16@itu.edu.tr, http://www.orcid.org/0000-0003-2429-0025
[2] *Istanbul Technical University, Department of Astronautical Engineering, 34469 Sariyer, Istanbul, Turkey*, celikbay@itu.edu.tr, https://orcid.org/0000-0002-7025-6330

Article Info

Received: *September 21, 2020*
Accepted: *December 08, 2020*
Online: *January 25, 2021*

Keywords: Hypersonic, High Enthalpy, OpenFOAM, Two-Temperature Model, Non-equilibrium Flows

Abstract

An implementation of a thermally non-equilibrium modeling on an existing open-source CFD solver is presented in this study. A newly coded open-source Navier-Stokes solver, *hyperReactingFoam*, including two-temperature model was developed within the framework of OpenFOAM. Disregarding electronic states in ionizing flows, the solver decomposes equilibrium temperature into trans-rotational and vibrational temperatures in thermal non-equilibrium conditions. Relaxations between distinct energy pools are achieved by utilizing an additional vibrational energy equation for each specie in the mixture. Coupling between trans-rotational and vibrational energy modes is governed by Landau-Teller equation. For energy transfers between different vibrationally excited species, formulation that is proposed by Knab et al. is implemented into the solver. The chemistry-vibrational coupling is realized by the Park TTv Model. Due to the multi-component nature of reacting flow, mixture pressure is calculated by using Dalton's Law from partial pressures of each reacting specie. Code validation tests are conducted on frequently used benchmark models such as adiabatic heat bath, blunted cone, and double cone models. It has been shown that *hyperReactingFoam* solver is in good agreement with other numerical solvers and experiments available in the literature.

To Cite This Article: D. Vatansever, B. Çelik, "An Open-Source Hypersonic Solver For Non-equilibrium Flows", Journal of Aeronautics and Space Technologies, Vol. 14, No. 1, pp. 35-52, Jan. 2021.

Denge Konumundan Uzak Akışlar İçin Açık Kaynak Kodlu Hipersonik Bir Çözücü

Makale Bilgisi

Geliş: *21 Eylül 2020*
Kabul: *08 Aralık 2020*
Yayın: *25 Ocak 2021*

Anahtar Kelimeler: Hipersonik, Yüksek Entalpi, OpenFOAM, İki-Sıcaklık Modeli, Denge Konumundan Uzak Akışlar

Öz

Bu çalışmada ısıl dengede olmayan tepkimeli bir akış çözücüsü mevcut açık kaynaklı bir HAD çözücüsü modifiye edilerek geliştirilmiştir. Geliştirilen Navier-Stokes çözücüsü olan *hyperReactingFoam* OpenFOAM yazılımı kapsamında geliştirilmiş olup iki-sıcaklık modelini ihtiva etmektedir. İki sıcaklık modeli kapsamında, elektronik ve iyonlaşma etkileri ihmal edilerek ısıl dengeden uzak akış fiziği, denge sıcaklığının öteleme-dönme ve titreşimsel sıcaklıklara ayrılmasıyla modellenmiştir. Titreşimsel sıcaklıkların elde edilebilmesi adına korunum denklemlerine ek bir titreşimsel enerji denklem seti ilave edilmiştir. Öteleme-dönme ve titreşimsel enerji modları arasındaki rahatlama etkisi Landau-Teller denklemi ile, farklı titreşimsel modlar arasındaki enerji transferleri Knab vd. tarafından geliştirilen bir formülasyon ile, kimyasal etkilerle titreşimsel enerji modu arasındaki etkileşim ise Park TTv modeli ile gerçekleştirilmiştir. Karışımın toplam basıncı Dalton yasası yardımıyla hesaplanmıştır. Geliştirilen çözücü adyabatik ısı banyosu, küt burunlu koni ve sivri burunlu koni gibi hipersonik problemlerde sıklıkla kullanılan test modelleri üzerinde doğrulanmıştır. Doğrulama çalışmalarından elde edilen sonuçlara göre *hyperReactingFoam* çözücüsünün literatürdeki diğer hipersonik çözücüler ve deneyler ile uyumlu olduğu görülmüştür.

NOMENCLATURE

$\mathbf{R}$	=	gas constant
$\boldsymbol{\rho}$	=	density
$\mathbf{c_v}$	=	specific heat at constant volume
$\mathbf{c_p}$	=	specific heat at constant pressure
$\mathbf{C_p}$	=	pressure coefficient
$\mathbf{C_f}$	=	friction coefficient
$\mathbf{Y}$	=	mass fraction
$\mathbf{X}$	=	molar fraction
$\mathbf{e}$	=	internal energy per unit mass
$\mathbf{M}$	=	molecular weight
$\mathbf{n_{m,s}}$	=	number density of the colliding pair
$\mathbf{c_m}$	=	average molecular speed
$\boldsymbol{\sigma_{v,m}}$	=	limited collision cross- section
$\mathbf{u}$	=	velocity component in x direction
$\mathbf{v}$	=	velocity component in y direction
$\mathbf{w}$	=	velocity component in z direction
$\boldsymbol{\delta}$	=	kronecker delta

SUBSCRIPTS

$\mathbf{t}$	=	translational
$\mathbf{r}$	=	rotational
$\mathbf{v}$	=	vibrational
$\mathbf{tr}$	=	trans-rotational
$\mathbf{s}$	=	specie index
$\mathbf{m}$	=	molecule index
∞	=	freestream value

1. INTRODUCTION

High speed vehicles re-entering atmosphere of a planet experience a combination of complex physical behaviors such as shock-wave interactions, chemical reactions and ionization processes. During a mission through an atmosphere, a re-entry craft travels through a number of different degree of rarefied environments ranging from the continuum to the free-molecular regime, for which distinct mathematical models are required [1]. Generally, these rarefied regions are classified in three parts: continuum regime, continuum-transition regime and free molecular regime [2].

The degree of rarefaction of a medium that a craft traverses is gauged by the Knudsen number, Kn. Mathematically, the Knudsen number represents the ratio of mean free path, that is an average distance between the colliding particles, to the characteristic length of flow [3]. The higher magnitude of this ratio specifies that hypersonic vehicle travels in the upper layer of atmosphere, which is characterized by low density, free-molecular regime (Kn >1), where the collisions of air molecules become rarer. At denser atmosphere, however, characteristic length of flow spans the maximum distance between colliding molecules, resulting in a lower value of Knudsen number (Kn < 0.2). Within this lower range, continuum approach can be adopted through the use of Navier-Stokes equations. Between 0.2 < Kn < 1.0, there is a transitional flow regime, where the collision impacts on vehicle's surface become important to capture the true nature of flow.

In order to extend the applicability of Navier-Stokes equations for continuum-transition regime, a two-temperature formulation [4] were offered by Park. In hypersonic speeds, the two-temperature formulation models thermally non-equilibrium flow. For high speeds, shock wave interactions cause high temperatures, at which internal energies of gases are characterized by distinct energy modes, which are representation of various motions in molecular level. These energy modes are translational, rotational, vibrational and electronic modes. The two-temperature model assumes that there are only two different temperatures associated with these energy modes. The first temperature, T_{tr}, is the equilibrium state of translational and rotational energies, whereas the second one, T_{ve}, is assumed to be equilibrium temperature of vibrational and electronic energies [5].

Even though the two-temperature model is applicable for a variety of problems, some objections are also addressed to the irrationality of the model. For instance, the deviation of rotational temperature from translational temperature of heavy particles is not recognizable in the model. Besides, in ionization processes radiation absorption effects cannot be included. The two-temperature model is unable to simulate some applications such as Martian and Titan entries, rarefied plume flows of rockets and, radio blackout problems [5].

There exist some numerical solvers capable of simulating hypersonic flows in the literature. DPLR and LAURA codes [6] developed by NASA were two of hypersonic solvers that can successfully calculate hypersonic flow properties around flying objects. DPLR code is a three-dimensional structured finite volume Navier-Stokes solver with reaction kinetics, thermal and chemical non-equilibrium flow physics implemented. The implicit time integration method "Data-Parallel Line Relaxation" implemented into the solver gives the name for DPLR code. In DPLR, Steger-Warming flux splitting [7] scheme for calculating inviscid fluxes was used with MUSCL extrapolation technique. The code achieves a third order spatial accuracy with a minmod limiter coupled to MUSCL extrapolation [8]. In LAURA, thermal non-equilibrium effects for reacting flows can also be simulated. Unlike DPLR, LAURA uses either point or line implicit time integration scheme in order to achive steady state. Inviscid fluxes are calculated with the help of Roe's average [9] and Harten's fixed entropy [10] schemes with Yee's symmetric TVD limiter [11].

Researchers from University of Minnesota developed another hypersonic code US3D [6]. US3D code

acquired much of its capability from the development stages of DPLR solver. While the codes generated by NASA are suitable for structured mesh only, US3D is able to perform unstructured mesh solutions as well. All of these three codes employ the two-temperature model in order to represent thermally non-equilibrium flows. In the case of reacting computation, ionization processes and dissociation reactions are taken into account in these three solvers. Another hypersonic non-equilibrium finite volume code called LEMANS [12] was developed by the University of Michigan. Similar to DPLR, numerical fluxes between adjacent cells are handled by Stegger-Warming flux splitting scheme. Two-temperature model
accounts for thermal non-equilibrium conditions. Time marching is achieved by a point implicit technique. hy2Foam [13] is an open-source CFD solver which is able to compute non-equilibrium hypersonic flows. With the help of the two-temperature model, hy2Foam has the capability to represent the energy transfers between different energy modes in reacting mixtures. Flux interpolations between neighbor cells are handled through the use of central-upwind scheme proposed by Kurganov, Noelle and Petrova [14]. dsmcFoam [15] and MONACO [16] codes include the implementation of DSMC method for rarefied re-entry problems for thermally and chemically non-equilibrium flow. rhoCentralFoam, which is an open-source code developed within the framework of OpenFOAM, is capable of solving thermal equilibrium, low enthalpy flows in hypersonic regime. With the help of rhoCentralFoam, both time accurate and time periodic low enthalpy solutions on hypersonic regime were obtained for a double wedge model by Durna et al. [17-18]

1.1. Objective

The objective of this study is;

- To develop and test a thermally non-equilibrium hypersonic solver that includes the two-temperature model,
- To include reacting capability on an existing open-source supersonic solver, *rhoCentralFoam*, in order to investigate the effect of chemistry on shock-shock and shock – boundary layer interactions,
- To compare the differences between reacting and non-reacting states of the solver for the continuum region,

The present solver does not contain electronic energy mode, hence disregards the ionization processes on high speed flows. In the development process of *hyperReactingFoam*, the standard structure of two existing solvers, *rhoCentralFoam* and *reactingFoam*, were preserved to a large extent. Without the necessity of a new library compilation, only minor modifications were made on the dependent libraries of these two existing solvers. In this regard, *hyperReactingFoam* provides other developers with the opportunity of improving the hypersonic solver easily. The solver provides an alternative to the literature for the solution of hypersonic problems by combining two existing solvers without making any major modification on the structures of OpenFOAM solvers and libraries.

2. METHODOLOGY

2.1. Governing Equations

Unsteady compressible reacting flows for thermal nonequilibrium can be solved using the Navier-Stokes-Fourier equations with continuum approach [19]. In these set of equations, mixture and individual specie densities are computed from total continuity and specie continuity equations, respectively. In addition to momentum equations and total energy equation, vibrational energy equations for each molecule in the mixture must also be solved. Because the electronic mode of energy is neglected in this study, all the terms related to this mode are dropped from original governing
equations. Thus, in vectorial form these equations can be written as:

$$\frac{\partial \boldsymbol{U}}{\partial t} + \frac{\partial (\boldsymbol{F}_{i,inv} - \boldsymbol{F}_{i,vis})}{\partial x_i} = \dot{\boldsymbol{W}} \qquad (1)$$

where $\mathbf{F}_{i,inv}$ and $\mathbf{F}_{i,vis}$ represent inviscid and viscid flux vectors, respectively whereas $\dot{W}$ shows source vector. Primitive vector, **U**, is stated as:

$$\boldsymbol{U} = \left[\rho, \rho_s, \rho u, \rho v, \rho w, E_{v,m}, E\right]^T, \quad s \in N_s, \quad m \in N_m \qquad (2)$$

where N_s and N_m represent the total number of species and the total number of molecules in the mixture, respectively. Inside the primitive vector, ρ and ρ_s symbolize total density of the mixture and partial density of s^{th} specie in the mixture, respectively. u, v, and w are the velocity components in x, y and z directions in the Cartesian coordinate system, respectively. $E_{v,m}$ and E indicate total vibrational energy of m^{th} molecule in the mixture and total energy of the flow, respectively. The flux vectors are divided into two contributions as inviscid and viscid parts and stated as:

$$\boldsymbol{F}_{i,inv} = \begin{bmatrix} \rho u_i \\ \rho_s u_i \\ \rho u_i u + \delta_{i1} p \\ \rho u_i v + \delta_{i2} p \\ \rho u_i w + \delta_{i3} p \\ E_{v,m} u_i \\ (E + p) u_i \end{bmatrix} \qquad (3)$$

$$\boldsymbol{F}_{i,vis} = \begin{bmatrix} 0 \\ J_{s,i} \\ \tau_{i1} \\ \tau_{i2} \\ \tau_{i3} \\ -q_{v,i,m} - e_{v,m} J_{m,i} \\ \tau_{ij} u_j - q_{tr,i} - q_{v,i} - \sum_s h_s J_{s,i} \end{bmatrix} \quad (4)$$

In Eq. (3) and Eq. (4), both i and j specifies one of three dimensions in Euclidian space. In Eq. (3), δ is the Kronecker delta function whereas p is the total pressure of the mixture, whose unit is in Pascal (Pa). The second row in $F_{i,inv}$ shows s^{th} specie's inviscid mass flux through the cell faces whereas the sixth row indicates the inviscid vibrational energy flux through the cell faces. In $F_{i,vis}$, the second row illustrates s^{th} specie's mass diffusion flux. In the sixth row, the first term represents vibrational conductivity due to vibrational energy gradient in the flow domain while the second term indicates vibrational energy transfer due to species' mass diffusion. In the last row, q_{tr} and q_v are heat conduction terms due to the gradient of trans-rotational and vibrational temperatures in the flow domain. The last term in this row includes diffusion of species' enthalpies which contains chemical related information. h_s shows the enthalpy per unit mass of s^{th} specie. J_s and J_m represent the mass diffusion fluxes of s^{th} specie and m^{th} molecule in the mixture, respectively.

Total pressure, p, is obtained from the partial pressure, p_s, of each reacting species through Dalton's Law:

$$p = \sum_s p_s = \sum_s \rho_s R_s T_{tr} \quad (5)$$

where T_{tr} and R_s show trans-rotational temperature and specific gas constant of species s, respectively. In Eq. (4), shear stress tensor is represented by τ_{ij} as following:

$$\tau_{ij} = \mu \left(\frac{\partial u_i}{\partial x_j} + \frac{\partial u_j}{\partial x_i} \right) + (\lambda + \mu_b) \frac{\partial u_k}{\partial x_k} \delta_{ij} \quad (6)$$

where Stokes' hypothesis holds such that second viscosity, λ and shear viscosity, μ are dependent variables with the relation $\lambda = -2/3\ \mu$, whereas bulk viscosity $\mu_b = 0$. The calculation of trans-rotational and vibrational heat conduction terms follows Fourier's law:

$$q_{tr,i} = \sum_s q_{tr,i,s} = \sum_s -\kappa_{tr,s} \frac{\partial T_{tr}}{\partial x_i}, \quad (7)$$

$$q_{v,i} = \sum_s q_{v,i,s} = \sum_s -\kappa_{v,s} \frac{\partial T_{v,s}}{\partial x_i} \quad (8)$$

where $T_{v,s}$ is vibrational temperature of species s. Calculations of trans-rotational, $\kappa_{tr,s}$ and vibrational, $\kappa_{v,s}$ thermal conductivities for s^{th} specie can be obtained from Eucken relation [20]:

$$\kappa_{tr,s} = \mu_s \left(\frac{5}{2} c_{vt,s} + c_{vr,s} \right), \quad \kappa_{v,s} = \eta_v \mu_s \quad (9)$$

where the coefficient $\eta_v = 1.2$ is predicted from kinetic theory [21]. $c_{vt,s}$ and $c_{vr,s}$ are s^{th} specie's specific heats at constant volume for translational and rotational modes, respectively. $c_{vt,s}$ and $c_{vr,s}$ can easily be derived from Eq. (26) and Eq. (27) by applying $c_{vt,s} \equiv (\partial e_{t,s}/\partial T_{tr})$ and $c_{vr,s} \equiv (\partial e_{r,s}/\partial T_{tr})$, respectively. Eucken relation produces satisfactory results only up to 6000 K temperatures. For better accuracy at even higher temperatures other refined approach should be used. The pure specie viscosity is found out by viscosity model proposed by Blottner et al. [22]:

$$\mu_s = 0.1\, e^{[(A_s ln T + B_s) ln T + C_s]} \quad (10)$$

where A_s , B_s, and C_s coefficient are specified for each reacting specie in the mixture. Mixture thermo-physical quantities are recovered from specie properties using Wilke mixing rule [23]. It is assumed that diffusion flux of each species is calculated through the gradient of the mass fraction. Diffusion flux among a mixture of similar particles can be calculated through [19]:

$$J_{s,i} = \rho D_s \frac{\partial Y_{s,i}}{\partial x_i} \quad (11)$$

where Y_s shows mass fraction of species s. Constant Lewis number, Le, approximation [19] is used to determine the diffusion coefficient of species s, D_s:

$$Le = \frac{D_s}{\alpha} = \frac{\rho D c_p}{\kappa} \quad (12)$$

where α, D, c_p and κ represent mixture averaged values of trans-rotational thermal diffusivity, diffusion coefficient, specific heat at constant pressure and thermal conductivity, respectively. Eq. (12) states that all the species in the mixture have the same diffusion coefficient, D. In Eq. (12), constant Lewis approximation is assumed and in this regard, a constant Le number, 1.4, is accepted. Nevertheless, constant Lewis approximation for diffusion coefficient calculation cannot yield satisfactory results for higher Knudsen, Kn, numbers in atmospheric entries, especially for ionization processes. The right hand side vector of Eq. (1) is composed of source terms:

$$\dot{\boldsymbol{W}} = [0, \dot{w}_s, 0, 0, 0, \dot{w_{v,m}}, 0]^T \quad (13)$$

where $\dot{w}_s$ is the net mass production of specie s and $\dot{w_{v,m}}$ is the energy source for the molecule $m \in N_m$. Definition for vibrational source term is as follows:

$$\dot{w_{v,m}} = Q_{m,V-T} + Q_{m,V-V} + Q_{m,C-V} \quad (14)$$

In this equality, indices V−T, V−V, C−V represent the energy transfer between vibrational - trans-rotational,

vibrational - vibrational, and chemistry - vibrational modes, respectively. Energy exchange between vibrational and trans-rotational energy modes is governed by Landau-Teller equation [24], which can be expressed in the following form:

$$Q_{m,V-T} = \rho_m \frac{e_{v,m}(T_{tr}) - e_{v,m}(T_{v,m})}{\tau_{m,V-T}} \quad (15)$$

where $\tau_{m,V-T}$ is the molar averaged relaxation time between vibrational and trans-rotational modes. This quantity is calculated from Millikan and White semi-empirical correlation [25] with Park's correction factor [26]:

$$\tau_{m,V-T} = \frac{\sum_s X_s}{\sum_s X_s/\tau_{m-s,V-T}} \quad (16)$$

where Landau-Teller inter-species relaxation time [19] $\tau_{m-s,V-T}$ is expressed by the function:

$$\tau_{m-s,V-T} = \frac{1}{p}\exp\left[A_{m,s}\left(T_{tr}^{-1/3} - B_{m,s} - 18.42\right) + \frac{1}{\overline{c_m}\sigma_{v,m}\, n_{m,s}}\right] \quad (17)$$

where the unit of p in Eq. (17) is in the standard atmosphere (atm). Coefficients $A_{m,s}$ and $B_{m,s}$ can be calculated from equations provided in [13]. The second term of this correlation is the collision-limited relaxation time offered by Park [26]. In Eq. (17), $n_{m,s}$ shows the number density of the colliding pair (m,s), $\overline{c_m}$ indicates the average speed of m^{th} molecule and $\sigma_{v,m}$ is the limited collision cross section area of m^{th} molecule, which are formulated by as follows:

$$\overline{c_m} = \sqrt{\frac{8R_m T_{tr}}{\pi}} \quad (18)$$

$$\sigma_{v,m} = \sigma_m \left(\frac{50{,}000}{T_{tr}}\right)^2 \quad (19)$$

In Eq. (18), R_m is the specific gas constant of molecule m. In Eq. (19), σ_m is taken as 3.0 x 10^{-21} m^2 for N_2 and O_2, and is set to 3.0 x 10^{-22} m^2 for NO [27]. $Q_{m,V-V}$ is modelled according to the relation proposed by Knab et al [28-29]. Chemistry-vibrational coupling is operated through Park TTv model, in which the representing term $Q_{m,C-V}$ takes the following form [30]:

$$Q_{m,C-V} = \dot{w}_m D'_m \quad (20)$$

where the coefficient D'_m m is obtained from a preferential model [31]:

$$D'_m = \alpha_m D_m \quad (21)$$

where the dissociation potential for each specie m , D_m, is a specie thermodynamic property whereas the dissociation energy constant, α_m, is typically assumed to be 0.3 [19]. The reaction source written in the second row in the right hand side of Eq. (13) can be expanded as:

$$\dot{w}_s = M_s \sum_{r=1}^{N_r} (\, v''_{s,r} - v'_{s,r}\,)\, x \left[k_{f,r} \prod_{k=1}^{N_r} \left(\frac{\rho_k}{M_k}\right)^{v'_{k,r}} - k_{b,r} \prod_{k=1}^{N_r} \left(\frac{\rho_k}{M_k}\right)^{v''_{k,r}}\right] \quad (22)$$

Here $v'_{s,r}$ and $v''_{s,r}$ denote forward and backward stoichiometric coefficients for each specie in the mixture while N_R is the number of reactions. M_s is the molecular weight of species s whereas $k_{f,r}$ and $k_{b,r}$ are the forward and backward reaction rates of r^{th} reaction, respectively. Both forward and backward reaction rates require the use of Arrhenius law and the use of trans-rotational temperature:

$$k_{f,r} = A\ x\ {T_{tr}}^{\beta}\ x\ \exp\left(-\frac{T_a}{T_{tr}}\right) \quad (23)$$

where forward rate constants A , β, and T_a represent a pre-exponential factor, temperature exponent and activation temperature, respectively. The value of β for any reaction can be determined by fitting the Arrhenius equation to the experimental data. In the present study, the value of β changes between -1.1 and 0.0 for the chemistry model provided in Table 9 and takes a value of -1.6 when single step dissociation of N_2 is considered.

2.2. Two-Temperature Model

The sum of kinetic, translational, rotational, vibrational, and chemical energies composes the total energy, E, as shown in Eq. (24) below:

$$E = \frac{1}{2}\rho \sum_i u_i^2 + \sum_s E_{t,s} + \sum_s E_{r,s} + \sum_s E_{v,s} + \sum_s \rho_s h_s^o \quad (24)$$

where h_s^o denotes the standard formation enthalpy of s^{th} specie in the mixture. Each of three energy pools, in thermal non-equilibrium, is described by a specific temperature. However, rotational and translational modes are specified by a single temperature, T_{tr}, since rotational energy mode relaxes quickly such that it can be assumed in thermal equilibrium with translational mode [32]. The energy per unit mass of any specie in the mixture can be related to total energy of a particular mode as following:

$$E_v = \sum_s E_{v,s} = \sum_s \rho_s e_{v,s} \quad (25)$$

The distinct internal energies per unit mass of species for each pool can be written as:

$$e_{t,s} = \frac{3}{2} R_s T_{tr} \quad (26)$$

$$e_{r,s} = R_s T_{tr} \quad (27)$$

$$e_{v,s} = R_s \left(\frac{\theta_{v,s}}{\exp\left(\frac{\theta_{v,s}}{T_{v,s}}\right) - 1.0}\right) \quad (28)$$

where $e_{t,s}$, $e_{r,s}$ and $e_{v,s}$ represent the internal energy per unit mass of species s for translational, rotational and vibrational modes, respectively. Vibrational characteristic temperature, $\theta_{v,s}$, is obtained from the implementation of simple harmonic oscillator model [32]. Summing up translational and rotational internal energies reorders Eq. (24) as:

$$E = \frac{1}{2}\rho \sum_i u_i^2 + E_{tr} + \sum_s E_{v,s} + \sum_s \rho_s h_s^o \qquad (29)$$

3. SOLVER DEVELOPMENT

Generated in C++ programming language, OpenFOAM benefits from finite volume numeric to solve the partial differential equations on any unstructured mesh. The new solver, *hyperReactingFoam*, was created with the help of two built-in standard solvers, *rhoCentralFoam* and *reactingFoam*, within the framework of OpenFOAM. Shock wave - boundary layer interactions for non-reacting supersonic or hypersonic flows can be predicted by *rhoCentralFoam*, which is a density based, open-source, cell centred, finite volume Navier-Stokes solver within OpenFOAM. *rhoCentralFoam* is able to produce non-oscillatory solutions in the presence of discontinuities such as shock waves and contact surfaces. *rhoCentralFoam* utilizes an operator splitting method to solve momentum and energy equations. In this method, "explicit predictor equations" for the convection of conserved variables are implemented while "implicit corrector equations" for the diffusion of primitive variables are used. In this way, explicit solution of convection part of equations with a diagonal solver provides fast convergence, while implicitly solved diffusion part of equations assists in terms of stability. The finite volume discretization used by *rhoCentralFoam* solver consists of semi-discrete, non-staggered central schemes for collocated variables assigned on polyhedral cells. Central-upwind scheme of Kurganov, Noelle and Petrova implemented in *rhoCentralFoam* produced successful results when validated against to analytical, numerical and experimental data in different type of problems [14].

In the cases of high temperatures, basic chemistry capabilities from *reactingFoam* solver are very useful because the influences of chemical reactions in re-entry problems cannot be ignored anymore. *reactingFoam* solver can store the specie properties in a pointer array, through which the development process of the new solver is tremendously eased. Nevertheless, *reactingFoam* can only produce low speed solutions and the numerics of the solver are not suitable for capturing shock wave interactions at high speeds.

In essence, *hyperReactingFoam* was developed by blending these two solvers on which some extra modifications applied. On the solver level, *hyperReactingFoam* include a specie transport equation and "m" number of vibrational energy equations for each molecule in the mixture. Mass fraction of each specie in the gas can be found from the former equation whereas vibrational temperature of each molecule can be obtained through the additional vibrational equations. In order to determine trans-rotational temperature, Eq. (29) was used to modify standard energy equation in *rhoCentralFoam*. By substracting Eq. (25) from Eq. (29) allows the solver to obtain trans-rotational temperature of heavy molecules. Central-upwind interpolation scheme of Kurganov, Noelle and Petrova was utilized for the discretization of additional vibrational energy equations. These vibrational energy equations, just as in the trans-rotational energy equation, are solved in two steps, which are composed of explicit predictor and implicit corrector equations. The calculation of reaction sources written in Eq. (22) is already available in *reactingFoam* solver. In order to compute reaction sources, array of specie names is introduced through a Chemkin [33] Interpreter input file. In addition to the list of reactants, the chemical reactions and the Arrhenius reaction rate parameters in Eq. (23) can also be introduced to the solver through the Chemkin file. The integration of reacting capabilities into *rhoCentralFoam* necessitates a library linking process. After linking the reaction libraries to the *rhoCentralFoam* solver, the capabilities of *reactingFoam* solver is thus activated and a combined solver, *hyperReactingFoam* can be generated. Figure 1 and Figure 2 depict general schematic diagram and algorithm of *hyperReactingFoam* solver, respectively.

Standard JANAF package in OpenFOAM libraries for the calculation of thermodynamic properties in relatively low temperatures has been extended to include a higher temperature range (200K - 20000K) [34] since the temperatures can exceed the default maximum limit provided in the library. The extended JANAF package include polynomial functions with 9 coefficients while, in unmodified state, JANAF package contain polynomial functions with 7 coefficients, which are only valid between 200 K – 6000 K. Furthermore, thermodynamic properties such as thermal conductivity and viscosity are incorporated into the solver as shown in Eq. (9) and Eq. (10). Moreover, Wilke's mixing rule for the calculation of mixture values is also externally added to the solver.

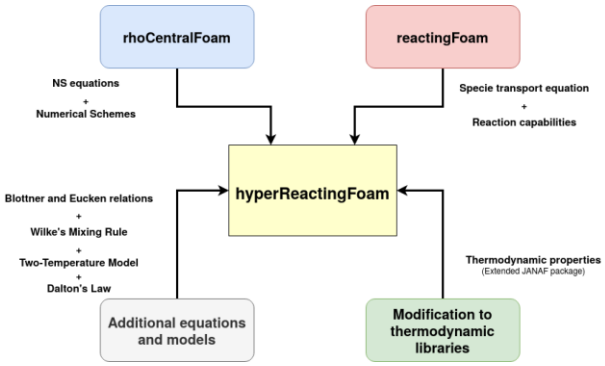

Figure 1. *hyperReactingFoam* schematic diagram for thermal non-equilibrium

Algorithm : *hyperReactingFoam* Solver

while $t < t_{end}$ **do**

- set $t = t + \Delta t$
- include viscosity, thermal conductivity model and Wilke's mixing rule
- evaluate surface fluxes for continuity, momentum and trans-rotational energy equations
- solve continuity
- solve explicit predictor equation for momentum
- update velocity field
- solve implicit corrector equation for momentum
- solve "s" number of specie transport equations for mass fractions
- solve explicit predictor equation for trans-rotational energy
- update trans-rotational temperature field
- solve implicit corrector equation for trans-rotational energy
- solve equation of state by Dalton's Law
- compute the relations required for the two-temperature model
- evaluate surface fluxes for vibrational energy equations
- solve "m" number of explicit predictor equations for vibrational energy
- update vibrational temperature field of each specie
- solve "m" number of implicit corrector equations for vibrational energy

end while

Figure 2. *hyperReactingFoam* solution algorithm for thermal non-equilibrium

4. SOLVER VALIDATION

In this section, validations of relaxation between distinct energy modes on three different benchmark models were presented. The test of *hyperReactingFoam* followed a validation process starting from simple to more complex cases and physics. Numerical solutions obtained from *hyperReactingFoam* for these benchmark models were compared against to other numerical solvers; *LEMANS*, *MONACO*, *hy2Foam*, and an experiment.

In stagnant conditions, an adiabatic heat bath represented by a cubic model whose side lengths are equal to $1x10^{-5}$ m was chosen. Computational domain for heat bath model consists of one cell only. Time step for each calculation in heat bath problems was set to be $1x10^{-9}$ s. Both reacting and non-reacting computations were performed on adiabatic heat bath. The relaxation process between vibrational and trans-rotational temperatures was investigated for both single species and two species mixture. In addition to vibrational-translational relaxation, the energy exchanges between vibrationally excited species were also considered by using two-temperature model for both reacting and non-reacting calculations. In the case of momentum flux, a double cone and a blunted cone model were investigated for hypersonic conditions. Reacting and non-reacting solutions were obtained on the double cone while only non-reacting computations were performed on the blunted cone. In all of reacting case validations, the term related to chemistry-vibration coupling, $Q_{m,C-V}$, was also activated in the vibrational energy equation.

4.1. Single Species V-T relaxation – Heat Bath

Relaxation behaviour of nitrogen gas with two different processes, namely vibrational heating and vibrational cooling, was investigated. In the first process, nitrogen gas reaches the equilibrium temperature with a lower initial vibrational temperature whereas in the second process with a lower initial trans-rotational temperature. Initial conditions regarding these two processes can be seen in Table 1.

Table 1. Initial conditions of V-T relaxation process for single species

Variable	Vibrational Heating	Vibrational Cooling
Vibrational temperature : Tv^{o}_{N2}	1000 K	10000 K
Trans-rotational temperature : T^{o}_{tr}	10000 K	3000 K
Pressure : p^{o}	1 atm	1 atm
Velocity : U^{o}	0 m/s	0 m/s

From Figure 3 it is seen that thermal equilibrium at 7623 K is achieved after around 10 µs in vibrational heat bath case whereas the relaxation time for vibrational cooling to reach 4972 K lasts at least 30 µs. It is clear that results obtained from *hyperReactingFoam* are in agreement with the solutions [35] obtained from *MONACO* solver for both vibrational heating and cooling processes.

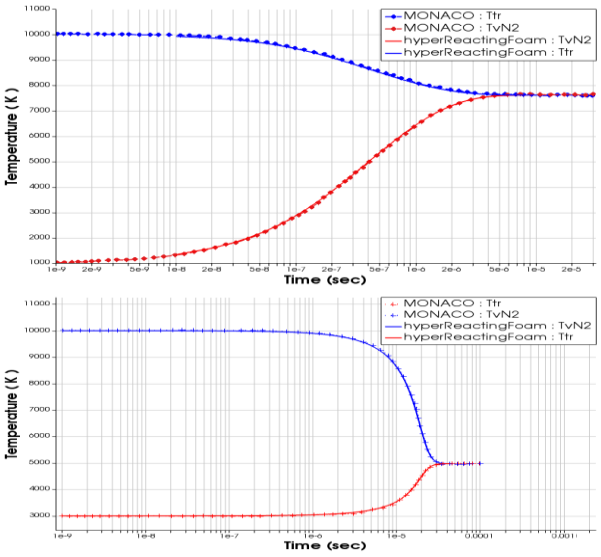

Figure 3. V-T thermal relaxation process for vibrational heating (top) and cooling (bottom) cases

4.2. Two Species V-T Relaxation For Non-reacting Mixture – Heat Bath

Differently from single specie relaxation, nitrogen atoms are also available in the mixture for this test case. The energy exchange occurs between vibrational and trans-rotational modes only since there are no any other molecule types other than N_2 in the mixture. At t=0, an equal amount of N_2 and N, in terms of number density, are existent in the adiabatic heat bath, for which the initial conditions are listed in Table 2. The number density for s^{th} specie in the mixture is defined as:

$$n_s = \frac{N_A}{M_s}\rho_s \tag{30}$$

where N_A denotes Avogadro constant.

Table 2. Initial conditions of V-T relaxation process for single species

Variable	Value	Unit
Vibrational temperature : Tv^o_{N2}	1000	K
Trans-rotational temperature : T^o_{tr}	30000	K
Number density for nitrogen molecules : n^o_{N2}	5 x 10^{22}	m^{-3}
Number density for nitrogen atoms : n^o_N	5 x 10^{22}	m^{-3}
Pressure : p^o	0.409	atm
Velocity : U^o	0	m/s

hyperReactingFoam result was validated against to *LEMANS* and *hy2Foam* solvers for this case . *hy2Foam* solver validated its own results against to *LEMANS* solver as well. The authors in [13] explains why their result is different from the solutions [35] obtained by *LEMANS* solver. As stated, they adopted a different convention for the second term of Eq. (17) in their study. In Figure 4, it is observed that *hyperReactingFoam* data overlaps with the results [13] obtained from *hy2Foam* solver, reaching the equilibrium temperature of 24350 K in approximately 2 µs.

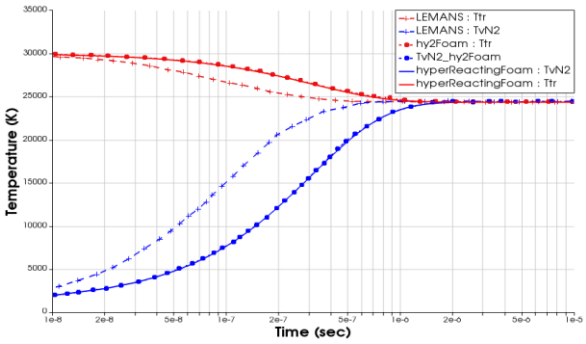

Figure 4. V-T thermal relaxation process for non-reacting N_2 – N mixture

4.3. Two Species V-T and V-V Relaxation – Heat Bath

In addition to vibrational-translational relaxations, now the energy transfer among different vibrationally excited species is also taken into account. This means that, in Eq. (14), the terms $Q_{m,V-T}$ and $Q_{m,V-V}$ were activated in order to simulate thermal relaxation process. It is assumed that the molecules N_2 and O_2 have initially equal vibrational temperatures in this vibrational cooling relaxation process. At the start of computation, the mass fractions of N_2 and O_2 were assumed to be equal to each other. The details regarding initial conditions for heat bath can be found in Table 3.

Table 3. Initial conditions of V-T and V-V relaxation process for N_2-O_2 mixture

Variable	Value	Unit
Vibrational temperature : Tv^o_{N2}	30000	K
Vibrational temperature : Tv^o_{O2}	30000	K
Trans-rotational temperature : T^o_{tr}	5000	K
Mass fraction of nitrogen molecules : Y^o_{N2}	0.5	-
Mass fraction of oxygen molecules : Y^o_{O2}	0.5	-
Pressure : p^o	1	atm
Velocity : U^o	0	m/s

Observation of the temperature variation graph in Figure 5 shows that O_2 molecules relax more quickly than N_2 molecules. It can be seen that both N_2 and O_2 reach thermal equilibrium at 12000 K after around 0.5 µs. It is understood that the results of *hyperReactingFoam* solver is closer to *hy2Foam* solver than *LEMANS* solver in this case since both *hy2Foam* and *hyperReactingFoam* can solve vibrational temperature of each species while *LEMANS* has only one vibrational temperature.

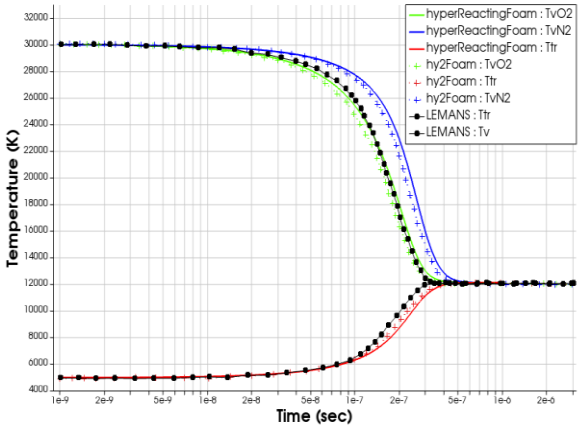

Figure 5. V-T and V-V thermal relaxation process between N_2 and O_2

4.4. Two Species V-T Relaxation For Reacting Mixture – Heat Bath

In this section, the effect of chemistry-vibration coupling term, $Q_{m,C-V}$, is tested as well as $Q_{m,V-T}$. This validation step tests whether the term $Q_{m,C-V}$ was implemented to the solver, correctly. For simplicity, only one step irreversible reaction was investigated. The reaction is the dissociation of nitrogen gas, whose Arrhenius parameters provided in Table 4 were taken from Park's Two-Temperature model [26].

$$N_2 + N_2 \overset{k_f}{\Rightarrow} 2N + N_2 \qquad (31)$$

Table 4. Arrhenius parameters for the calculation of reaction rates

Arrhenius Constants	A	β	T_a
Unit	$m^3\,mol^{-1}\,s^{-1}$	-	K
Value	7.0×10^{-21}	-1.6	113200

The verification was performed on the same heat bath model in which the initial number densities of N_2 and N were set to be equal as $5.0 \times 10^{22}\ m^{-3}$. At the start of computation, vibrational temperatures are in thermal non-equilibrium state with trans-rotational temperature.

The result of this case was compared against to *hy2Foam* solver, which adopts Park TTv model [36-37] for the solution showed in Figure 6. Variation of number densities of each reacting species was also compared on the same graph. Number density of each species is normalized with respect to the initial number densities at t = 0.

Table 5. Initial conditions of V-T and C-V relaxation process for reacting $N_2 - N$ mixture

Variable	Value	Unit
Vibrational temperature : Tv^o_{N2}	1000	K
Trans-rotational temperature : T^o_{tr}	30000	K
Number density for nitrogen molecules : n^o_{N2}	5×10^{22}	m^{-3}
Number density for nitrogen atoms : n^o_N	5×10^{22}	m^{-3}
Pressure : p^o	0.409	atm
Velocity : U^o	0	m/s

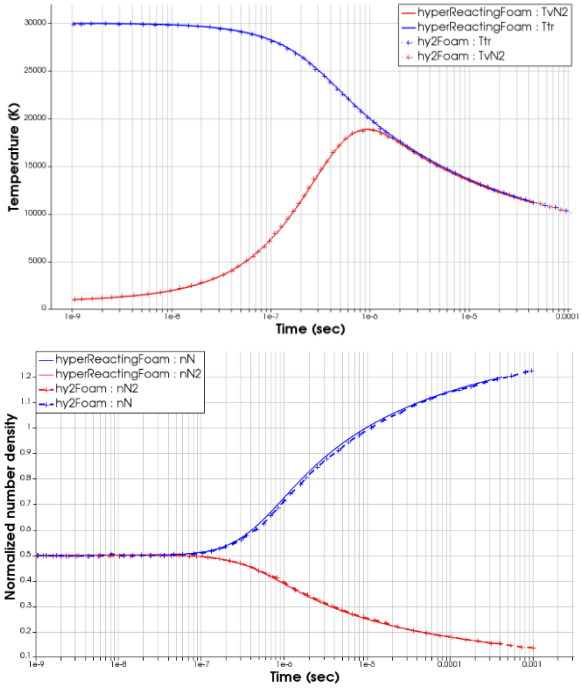

Figure 6. Thermal relaxation (top) and number density variation (bottom) for reacting N_2-N mixture

The comparison of Figure 4 and Figure 6 illustrates that although the required time to achieve thermal equilibrium state for both cases is reached within 2 μs, the values of equilibrium temperature are completely different from each other. In the reacting case, the equilibrium temperature is in a decreasing trend due to the chemistry-vibration coupling whereas the final temperature in the non-reacting case stays at a constant value even after thermal equilibrium state is satisfied. It is clear that the number densities of the reacting species still change even after thermal relaxation is completed. This indicates fact that N_2 molecules still keep dissociating irreversibly to produce N atoms.

4.5. Non-reacting V-T Relaxation On A Blunted Cone

Another case in which a thermally non-equilibrium condition can be investigated is a blunted cone model. For validation purposes, the exact computational model and the free-stream conditions were selected from the study of Brown et al. [1], in which the results of *hy2Foam* solver are published on the blunted cone. The computational domain for the blunted cone consists of fully structural elements with 600 in stream-wise and 200 in normal direction. The nose of the blunted cone with a radius of 6.35 mm is extended with a flat plate that has a length of 5 cm in the stream-wise direction. The cone surface has an angle of 25° with free-stream direction. The height of first cell thickness in the boundary layer mesh is around 10 μm.

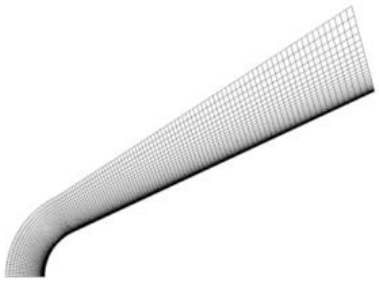

Figure 7. Computational domain for blunted cone model [1]

Unlike heat bath cases, there is now a free-stream flow over blunted cone. The free-stream flow contains N_2 molecules only. The free-stream conditions for nitrogen flow can be seen from Table 6. Mach number of free-stream flow is equal to 11.3. Maxwell slip [38] for velocity and Smoluchowski jump [39] condition for trans-rotational and vibrational temperatures were applied on the cone surface, respectively. Trans-rotational and vibrational temperatures of N_2 molecules were assumed to be in equilibrium at t=0. Time step for each iteration was calculated from the maximum Courant number of 0.5. The validation was again performed with the help of *hy2Foam* solver. The quantities obtained from *hyperReactingFoam* were compared against to the results both on stagnation line and cone surface [1].

Table 6. Initial conditions of non-reacting nitrogen flow on blunted cone model

Variable	Value	Unit
Free-stream velocity : U_∞	2764.5	m/s
Free-stream pressure : p_∞	21.9139	Pa
Free-stream density: ρ_∞	5.113×10^{-4}	kg/m^3
Free-stream temperature: T_∞	144.4	K
Free-stream mean-free-path: λ_∞	1.01×10^{-4}	m
Overall Knudsen number : Kn_{ov}	0.002	-
Wall temperature : T_w	297.2	K

Each quantity obtained on stagnation line was normalized with respect to its free-stream value provided in Table 6. In Figure 8, x-axis shows the axial distance on the stagnation line, whose endpoint is located at x=0. This location on the nose of the blunted cone, where the velocity goes to zero, is called as "stagnation point" for the viscid flows with no-slip conditions. At a shock stand-off distance of 1.1 mm, a detached bow shock occurs in front of the blunted cone as seen in the bottom-right frame of Figure 8. It is clear that the thickness of the shock is approximately 0.3 mm as there are steep jump and decrease in the density and velocity distributions within the interval of -1.1 mm < x < -0.8 mm. The temperature variation graph depicts that the thermal equilibrium state between trans-rotational and vibrational modes disrupts after passing through the normal shock. This trend is understandable because when a flow passes through strong discontinuities such as normal shocks, a great deal of its kinetic energy is converted to translational motion. This translational motion then exchanges its energy with rotational, vibrational and chemical energies within a certain number of collisions [19]. It is also observed that trans-rotational and vibrational energy modes are in thermal equilibrium at the stagnation point.

The definitions of pressure and friction coefficients are given by:

$$C_p = \frac{p - p_\infty}{0.5\,\rho_\infty\,U_\infty^2}\,, \tag{32}$$

$$C_f = \frac{\tau}{0.5\,\rho_\infty\,U_\infty^2}\,, \tag{33}$$

where τ shows shear stress of the fluid whereas p_∞, ρ_∞ and U_∞ are the free-stream values of pressure, density and velocity, respectively. Pressure and friction coefficients for both solvers were plotted on the same graph. The comparison between two solvers in Figure 9 shows that the surface coefficients are in well agreement.

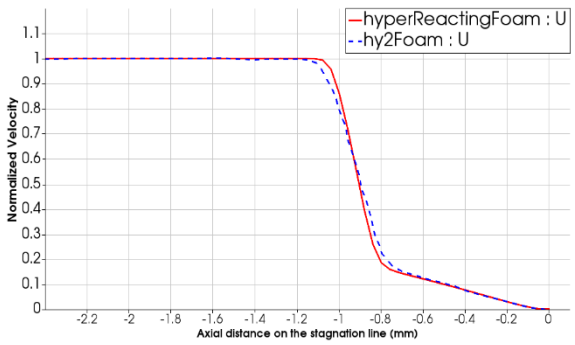

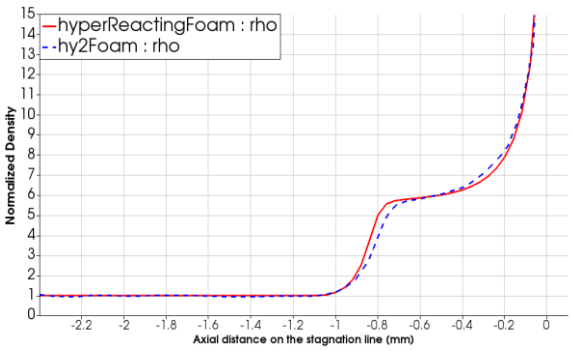

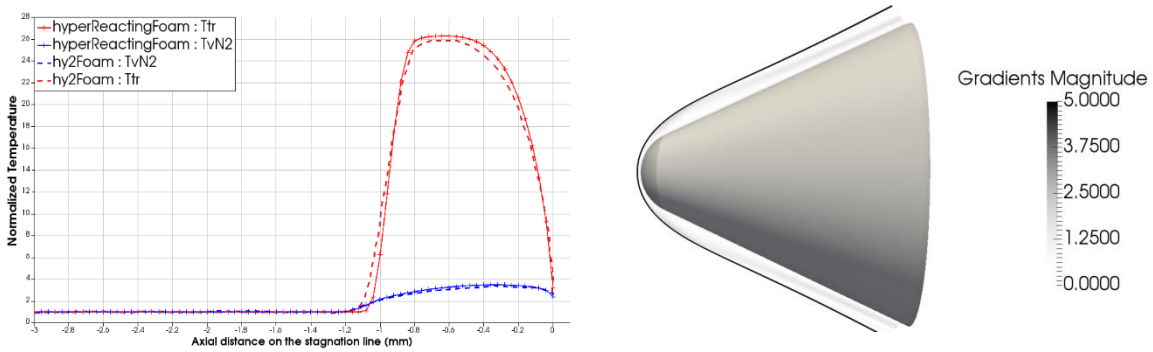

Figure 8. Prediction of velocity (upper-left), density (upper-right), temperature (bottom-left) profiles on the stagnation line and the density gradient contour (bottom-right) for the flow-field

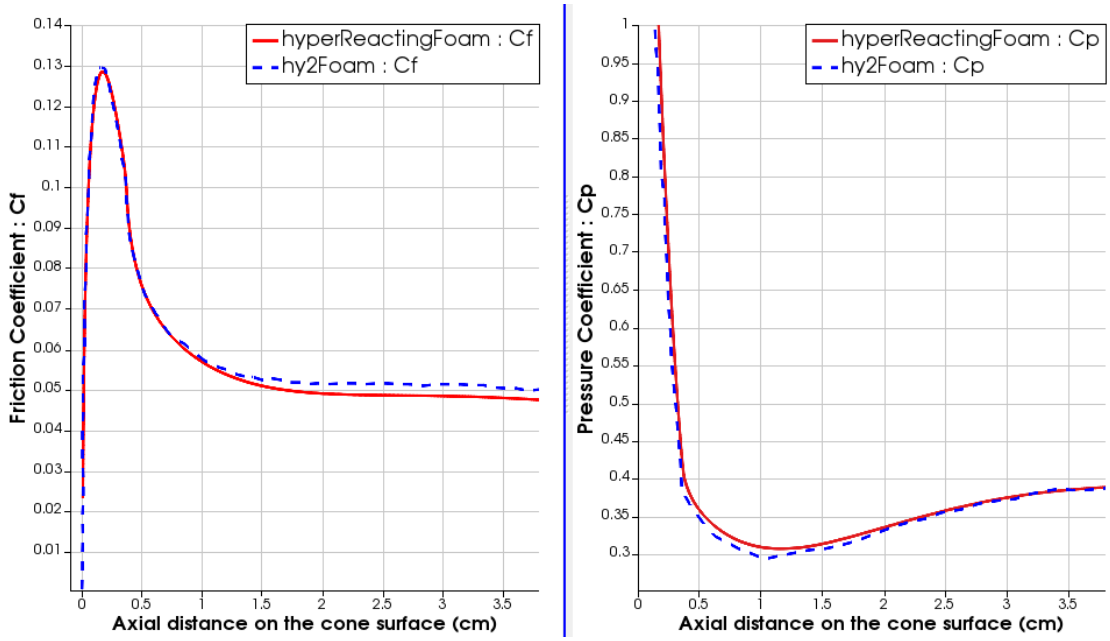

Figure 9. Prediction of pressure (left) and friction (right) coefficients on the cone surface

4.6. Non-reacting Validation On A Double Cone

Another model for verification of *hyperReactingFoam* is a double cone geometry on which low and high enthalpy experiments conducted in Calspan University of Buffalo Research Center (CUBRC)'s LENS XX expansion tunnel [40]. Thermally non-equilibrium capability of the solver was tested with the help of low enthalpy experiment for both non-reactive and reactive conditions performed on the double cone. In addition to the experiment, a numerical solution on the double cone model published by Kianvashrad and Knight [41] is also used to validate *hyperReactingFoam*. Surface heat flux and pressure distributions are used to compare the differences between experimental and numerical solutions. The picture and geometric dimensions of experimental model was given in Figure 10.

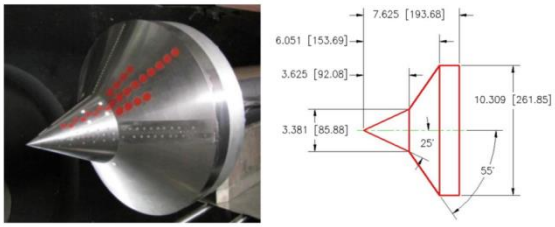

Figure 10. Double cone model used in low enthalpy experiment, dimensions in millimeters, courtesy of CUBRC

The first and second surfaces of double cone model make angles of 25° and 55° with free-stream direction, respectively. Table 7 provides experimental flow conditions of double cone model.

Table 7. Low enthalpy experimental flow conditions on double cone model

Variable	Value	Unit
Total enthalpy : h_o	9.65	MJ/kg
Pitot pressure	17.5	kPa
Unit Reynolds, 10^6/m	0.19	m^{-1}
Velocity	4303	m/s
Density	0.984	g/m^3
Temperature	389	K
Y_{N2}	0.765	-
Y_{O2}	0.235	-

Figure 11 illustrates the close-up picture of compression corner and boundary surfaces for the computational domain generated for comparison purpose. The computational domain consists of 32385 structural hexahedral elements. Due to non-catalytic wall condition, surface normal gradients of species' mass fractions were taken as zero (Neumann condition). On wedge surface, constant temperature condition for trans-rotational temperature and adiabatic condition for vibrational temperatures were applied. The trans-rotational wall temperature was assumed to be equal to isothermal wall temperature of 300 K at all times. Free-stream conditions of experiment provided in Table 7 were given as boundary conditions at Inlet surface whereas Neumann type boundary condition was assigned for all quantities at Outlet surface. Other types of boundary conditions can also be seen in Table 8.

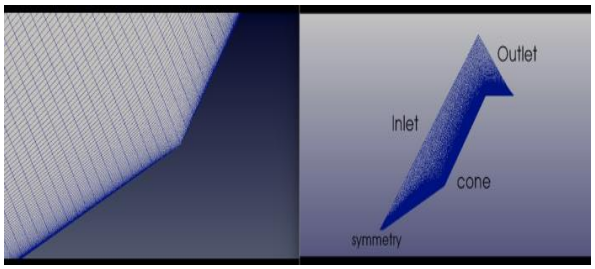

Figure 11. Structural elements and computational domain generated for the double cone model

wedge1 and wedge2 surfaces are the front and back sides of the computational domain. "wedge" and "symmetry" boundary condition types specify rotational symmetry of flow and the symmetry of flow with respect to the horizontal axis, respectively. Specie mass fractions at t=0 were taken as Y_{N2} = 0.76, Y_{O2} = 0.23, Y_{NO} = 0.01, Y_N = 0.0 and Y_O = 0.0 at every cell in the computational domain. Prandtl number was set to 0.736 [39]. Non-reacting solution for thermal non-equilibrium was compared both against to the experimental and a numerical study performed on the same double cone model.

Figure 12 illustrates the time variations of surface heat flux and pressure distributions on the cone surface. It can be seen that the solution approaches steady state after around 300 μs. When the steady state solution is compared against to the experiment, it is observed that non-reacting analyses of *hyperReactingFoam* under-predicts the location of peak pressure and heat flux values while over-predicting the maximum peak magnitudes.

Table 8. Boundary condition types assigned on different boundary surfaces of the double cone (ZG: Zero Gradient, FV: Fixed Value, sym: symmetry)

Boundary	Velocity	Pressure	Temperature	Mass frac.
Inlet	FV	FV	FV	FV
Outlet	ZG	ZG	ZG	ZG
cone	NS	ZG	FV(Ttr), ZG(Tvi)	ZG
symmetry	sym	sym	sym	sym
wedge1	wedge	wedge	wedge	wedge
wedge2	wedge	wedge	wedge	wedge

The analysis of Kianvashrad and Knight, as shown in Figure 13, also under-predicts the peak locations in spite of over-predicting the magnitudes. Yet, the authors state that these over-predictions are irrelevant since the experimental gauge spacing is as much as 50 times of the computational grid spacing near the peak location [41]. It is also obvious that both solvers cannot precisely pinpoint the location of separation shock features, which are represented by the sudden drop and jump in the heat flux and pressure distributions on the first surface.

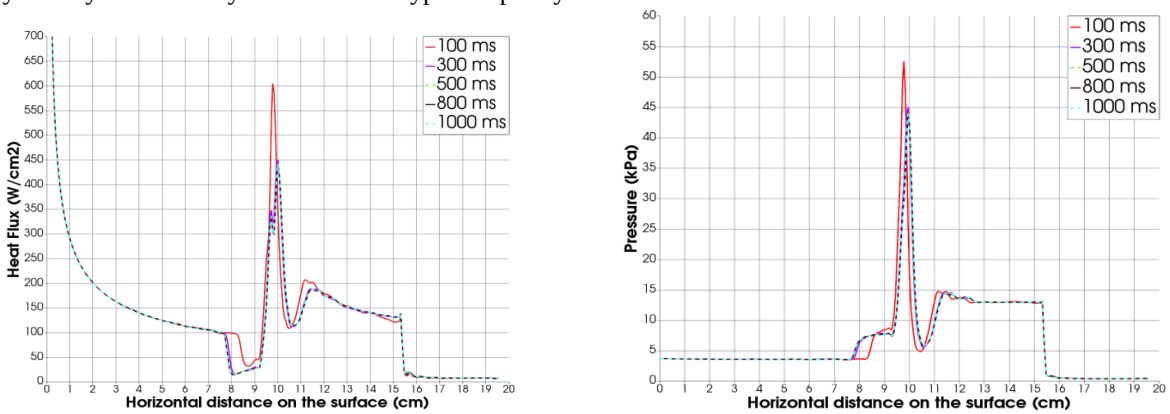

Figure 12. Time variations of surface heat flux (left) and pressure (right) distributions for non-reacting, thermal non-equilibrium flow

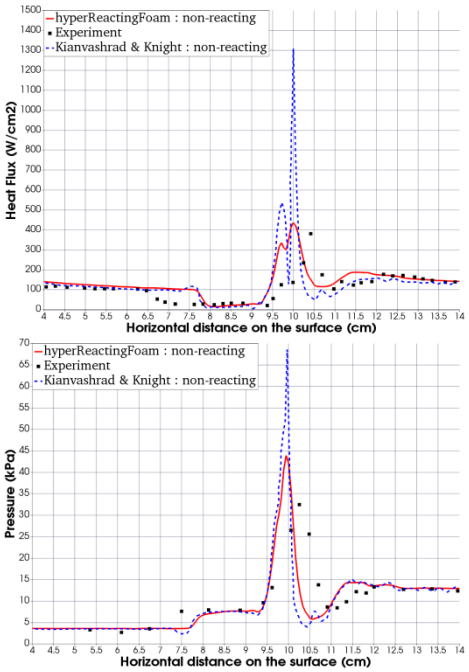

Figure 13. Surface heat flux (top) and pressure (bottom) distributions for non-reacting, thermal non-equilibrium flow

4.7. Reacting Validation On The Double Cone

Given the computational domain and boundary conditions stated in the previous section, the reacting solution on the double cone model can also be presented. For the reacting case, an air chemistry model [42] which is composed of 5 species (N_2, O_2, NO, N, and O) and 17 reactions was selected. The Arrhenius parameters for each chemical reaction can be read from Table 9.

Table 9. Thermo-chemistry model for the reacting air

Index	Reaction	A	β	T_a
		$m^3kmol^{-1}s^{-1}$	-	K
1	$O_2 + N_2 \rightarrow 2O + N_2$	7.829e16	-1.0	59370.6
2	O2 + N → 2O + N	6.624e16	-1.0	59370.6
3	O2 + NO → 2O + NO	6.624e16	-1.0	59370.6
4	O2 + O2 → 2O + O2	3.210e16	-1.0	59370.6
5	O2 + O → 2O + O	9.033e16	-1.05	59370.6
6	N2 + O → 2N + O	2.409e15	-0.54	113497.4
7	N2 + O2 → 2N + O2	9.033e15	-0.68	113497.4
8	N2 + NO → 2N + NO	9.033e15	-0.68	113497.4
9	N2 + N2 → 2N + N2	2.469e15	-0.62	113497.4
10	N2 + N → 2N + N	6.022e15	-0.68	113497.4
11	NO + N2 → N + O + N2	1.265e17	-1.0	75544.2
12	NO + O2 → N + O + O2	1.204e17	-1.0	75544.2
13	NO + NO → N + O + NO	6.022e16	-1.0	75544.2
14	NO + O → N + 2O	2.409e17	-1.1	75544.2
15	NO + N → O + 2N	2.409e17	-1.1	75544.2
16	NO + O → O2 + N	1.385e8	0.5	19693.6
17	N2 + O → NO + N	4.818e10	0.0	37482.4

Time variation graph of pressure and heat flux distributions in Figure 14 illustrate that the reacting case reaches steady state solution at a later time, which is around 500 μs. In addition, the reacting solution shows that the magnitudes of pressure and heat flux peaks are less than those of non-reacting case.

Figure 15 depicts how the steady state value of heat flux and pressure vary over the cone surface. It is clear that the location and magnitude of pressure peak are better predicted than those of non-reacting case. We should note that when the chemistry is activated, the location of pressure peak gets closer to that of experimental study.

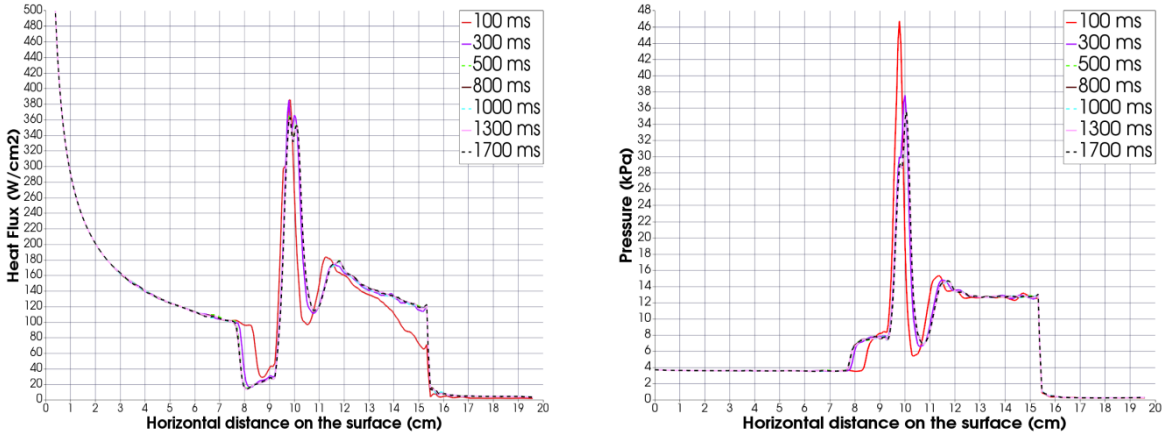

Figure 14. Time variations of surface heat flux (left) and pressure (right) distributions for reacting, thermal non-equilibrium flow

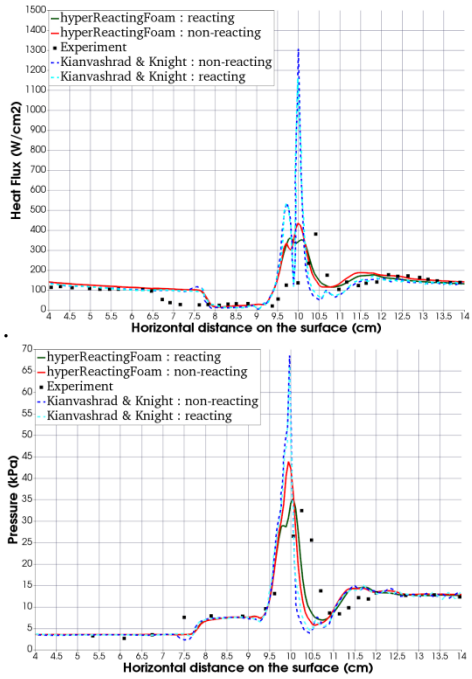

Figure 15. Surface heat flux (top) and pressure (bottom) distributions for reacting, thermal non-equilibrium flow

4.8. Comparisons Between Reacting and Non-reacting Solutions On The Double Cone Model

Figure 16 presents the time evolution and comparison of reacting and non-reacting numerical Schlieren images between 100 μs and 1000 μs. The blue lines represent the shock structures of reacting solution whereas the red lines show the shock structures of non-reacting solution over the double cone. The red contours on the cone surface specify the density gradient distribution of non-reacting solution. It is seen that at the tip of the cone, leading edge shock (LS) forms and this shock interacts with the separation shock (SS) formed due to boundary layer separation on the first surface. The result of this interaction causes another shock wave formation and this shock interacts at the triple point (TP) with the bow shock (BS) over the second surface. From TP, a transmitted shock (TS) impinges upon the second surface of the cone. We see that as the time progresses, an upstream movement of SS and a downstream movement of TS result in a larger separated region over the compression corner. It can be understood that apart from the BS, all the shock structures of both solutions overlap for all instants. After 400 μs, the distance between TPs of reacting and non-reacting solutions becomes more distinguishable.

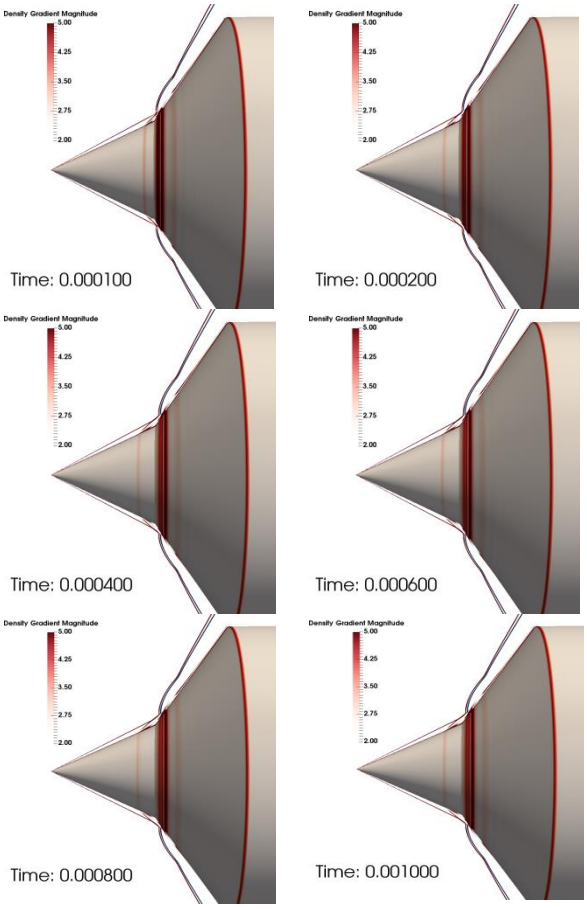

Figure 16. Time evolution of density gradient comparison between reacting (blue) and non-reacting (red) analyses on the double cone

Figure 17 shows the temperature and N_2 mass fraction contours for the reacting thermally non-equilibrium flow. Conspicuously, downstream locations of shock waves are the regions where the thermal equilibrium breaks down and the reactions become observable. Trans-rotational and vibrational temperatures reach the highest magnitudes around TP and the most upstream portions of BS. It is seen that when the flow passes through LS and SS, the relaxation between vibrational and trans-rotational temperatures is negligible as compared to downstream regions of BS, near compression corner and over the expansion surface. The maximum dissociation rate of N_2 in terms of mass fraction is observed to be around 0.05. A qualitative examination of the flow-field shows that the consumption of N_2 is insignificant over the first surface and near compression corner.

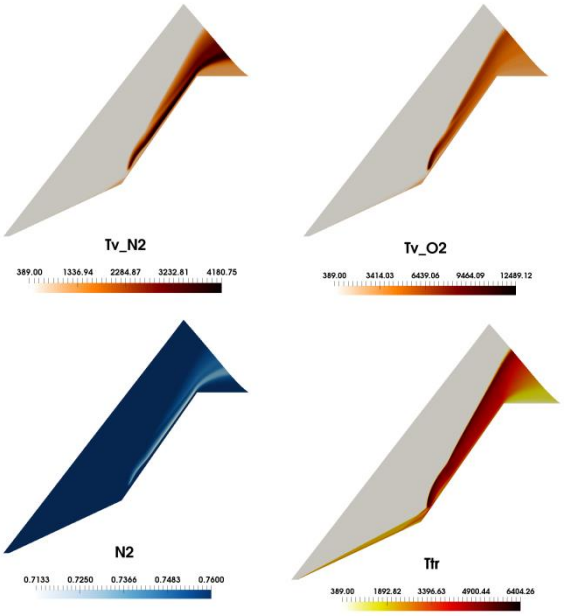

Figure 17. Tv_{N2}, Tv_{O2}, T_{tr} and N_2 contour distributions for the reacting, thermal non-equilibrium flow

Figure 18 depicts the differences between the thermal non-equilibrium nature of reacting and non-reacting flows on the cone surface. It is clear that the free-stream equilibrium temperature starts to break down after LS, where the reacting and non-reacting solutions overlap until the point of SS. The vibrational temperature of O_2 molecules on the wall always shows a larger magnitude than those of N_2 and NO molecules. We see that non-reacting analysis provides higher magnitudes of vibrational temperatures after x=10 cm, on which the maximum of pressures and heat fluxes are obtained.

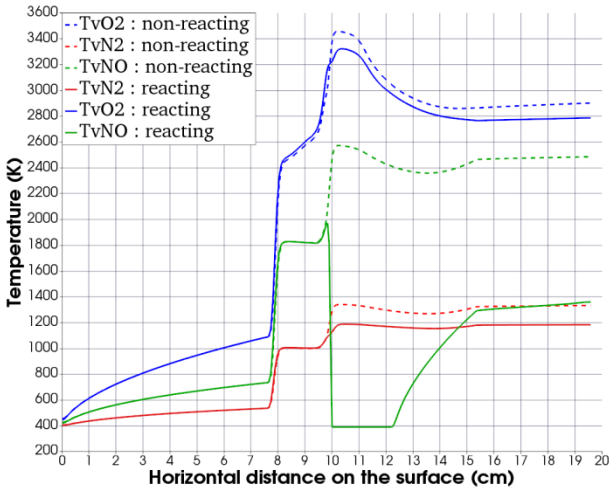

Figure 18. Comparison of reacting and non-reacting vibrational temperatures of N2, O2 and NO molecules on the cone surface

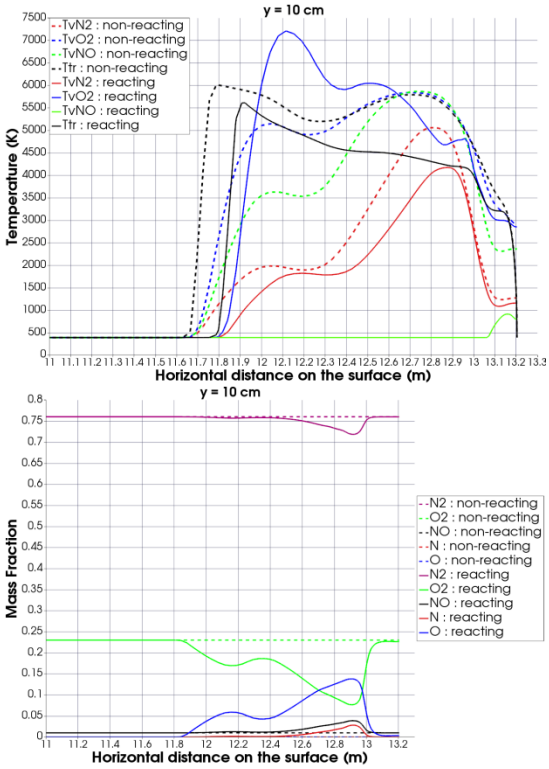

Figure 19. Reacting and non-reacting flow comparison for temperatures (top) and species mass fractions (bottom) over a line which is translated by 10 cm as parallel to the cone axis

Temperature and specie mass fraction distributions over a line in the flow-field are compared as shown in Figure 19. Obviously, thermal relaxation and chemical reactions start after passsing BS over the second surface. The differences between BS structures of reacting and non-reacting solutions observed in Figure 16 can also be understood from the temperature variations in Figure 19, where the thermal non-equilibrium of non-reacting analysis disrupts earlier than reacting analysis. Obviously, the slope of trans-rotational temperature distribution across SS is steeper than vibrational temperatures. It is seen that the maximum rate of creation and destruction of species occur at x=12.9 cm, where the existence of O atoms in the mixture increases up to 14 percent whereas the the consumption rate of O_2 molecules drops as much as 15 percent in terms of mass fraction. It is observed that the reactions nearly stop as the flow reaches on the cone surface.

5. CONCLUSION

An open-source hypersonic solver for thermally non-equilibrium flows were developed and tested for continuum and near-continuum regions, where Knudsen number is low and the continuum approach is adopted. The solver, *hyperReactingFoam* makes distinction between trans-rotational and vibrational temperatures. The solver implements the-two

temperature model of Park by disregarding the electronic modes, hence ionization processes. *hyperReactingFoam* was blended from two built-in solvers, *rhoCentralFoam* and *reactingFoam*. Chemistry-vibration coupling is integrated through Park TTv model. The solver offers testing of vibrational-transrotational and vibrational-vibrational temperature relaxations of multi-component mixtures for both non-reacting and reacting conditions. Validations of the newly - developed code were performed against to zero-dimensional and multi-dimensional benchmark cases. The testings showed that the solver is in well agreement with the numerical solvers and an experiment in the literature. *hyperReactingFoam* provides an alternative solver to the hypersonic community. The numerical computations of different hypersonic problems will also be investigated with thermal equilibrium and non-equilibrium for future works. Comparison analyses between reacting - nonreacting, thermal equilibrium - nonequilibrium, and continuum - rarefied conditions that can be done with the solver are expected to provide significant contributions to the hypersonic community.

6. ACKNOWLEDGEMENTS

This study was funded by the project of TUBITAK (215M907) and BAP (41944). Computing resources used in this work were provided by the National Center of High Performance Computing of Turkey (UHEM) under Grant No. 5004292016 and Grant No. 1006482019. In addition, the numerical computations reported in this paper were partially performed at TUBITAK ULAKBIM, High Performance and Grid Computing Center (TRUBA resources).

7. REFERENCES

[1] R. E. Brown, V. Casseau, D. E. R. Espinoza, and T. J. Scanlon, "A Two-Temperature Open-Source CFD Model for Hypersonic Reacting Flows, Part Two: Multi-Dimensional Analysis," *Aerospace 2016*, vol. 3, 2016. [Online]. Available: https://www.mdpi.com/2226-4310/3/4/45. [Accessed Sept. 20, 2020].

[2] A. J. Lofthouse, "Nonequilibrium Hypersonic Aerothermodynamics Using The Direct Simulation Monte Carlo And Navier Stokes Models", Ph.D. dissertation, The University of Michigan, Ann Arbor, MI, USA, 2008.

[3] J. D. Anderson, "*Hypersonic and High Temperature Gas Dynamics*", 2nd ed., *AIAA Education Series*, pp. 21-22, 2006.

[4] C. Park, "Assessment of Two-Temperature Kinetic Model for Ionizing Air," *Journal of Thermophysics and Heat Transfer*, vol. 3, no. 3, pp. 233–244, July 1989.

[5] C. Park, "The Limits of Two-Temperature Kinetic Model in Air", *48th AIAA Aerospace Sciences Meeting Including the New Horizons Forum and Aerospace Exposition, AIAA 2010, Orlando, Florida, USA, January 4 – 7, 2010*.

[6] M. Barnhardt, M. Wright, G. V. Candler, P. Gnoffo, B. Hollis, D. Hash, I. Nompelis, J. Olejniczak, M. Pulsonetti, and D. Prabhu, "FIRE II Calculations for Hypersonic Nonequilibrium Aerothermodynamics Code Verification: DPLR, LAURA, and US3D", *45th AIAA Aerospace Sciences Meeing and Exhibit, AIAA 2007 Reno, Nevada*, 2007.

[7] R. W. MacCormack, and G. V. Candler, "The Solution of the Navier–Stokes Equations Using Gauss–Seidel Line Relaxation," *Computers and Fluids*, vol. 17, no. 1, pp. 135–150, January 1989.

[8] H. C. Yee, "A Class of High-Resolution Explicit and Implicit Shock Capturing Methods," *NASA TM 101088*, Feb. 1989.

[9] P. L. Roe, "Approximate Riemann Solvers, Parameter Vectors and Difference Schemes," *Journal of Computational Physics*, vol. 43, no. 2, pp. 357-372, October 1981.

[10] A. Harten, "High Resolution Schemes for Hyperbolic Conservation Laws", *Journal of Computational Physics*, vol. 49, no. 3, pp. 357-393, April 1983.

[11] H. C. Yee, "On Symmetric and Upwind TVD Schemes," *NASA TM 88325*, 1990.

[12] L. C. Scalabrin, and I. D. Boyd. "Development of an unstructured navier-stokes solver for hypersonic nonequilibrium aerothermodynamics", *In Proceedings of the 38th AIAA Thermophysics Conference*, Toronto, ON, Canada, 6–9 June 2005.

[13] V. Casseau, R. C. Palharini, T. J. Scanlon, and R. E. Brown, "A Two-Temperature Open-Source CFD Model for Hypersonic Reacting Flows, Part One: Zero-dimensional Analysis", *Aerospace 2016*, vol 3, 2016 [Online]. Available: https://www.mdpi.com/2226-4310/3/4/34. [Accessed Sept. 20, 2020].

[14] A. Kurganov, S. Noelle, and G. Petrova, "Semi-discrete central-upwind schemes for hypersonic conservation laws and Hamilton Jacobi equations", *SIAM Journal on Scientific Computing*, vol. 23, pp. 707–740, 2001.

[15] D. E. R. Espinoza, V. Casseau, T. J. Scanlon, and R. E Brown, "An Open Source Hybrid CFD-DSMC Solver for High-Speed Flows", *In Proceedings of the AIP Conference*, Victoria, BC, Canada, 10–15 July 2016.

[16] I. D. Boyd, and Dietrich S., "Scalar and Parallel Optimized Implementation of the Direct Simulation Monte Carlo Method", *Journal of Computational Physics*, vol. 126, Issue 2, pp. 328-342, 1996.

[**17**] A. S. Durna, B. Celik, "Time-periodic shock interaction mechanisms over double wedges at Mach 7," *Shock Waves*, vol. 29, pp. 381–399, March 2019.

[**18**] A. S. Durna, B. Celik, "Effects of Double-Wedge Aft Angle on Hypersonic Laminar Flows", *AIAA Journal*, vol. 58, no 4, April 2020.

[19] G. V. Candler, and I. Nompelis, "Computational Fluid Dynamics for Atmospheric Entry, In Non-Equilibrium Dynamics: From Physical Models to Hypersonic Flights", *The von Karman Institute for Fluid Dynamics: Rhode-Saint-Genèse*, Belgium, 2009.

[20] W. G. Vincenti, and Jr., C. H. Kruger, *Introduction to Physical Gas Dynamics*, Krieger Publishing Company, Florida, 1965.

[21] J. Olejniczak, and G. V. Candler, "Vibrational Energy Conservation with Vibration - Dissociation Coupling: General Theory and Numerical Studies," *Physics of Fluids*, vol. 7, no. 7, pp. 1764-1774, July 1995.

[22] F. G. Blottner, M. Johnson, and M. Ellis, "Chemically Reacting Viscous Flow Program for Multi-Component Gas Mixtures," Sandia Laboratories, Report No. SC-RR-70-754, Albuquerque, New Mexico, 1971.

[23] C. R. Wilke, "A Viscosity Equation for Gas Mixtures", *Journal of Chemical Physics*, vol. 18, pp. 517-519, 1950.

[24] L. Landau, and E. Teller, "On the theory of sound dispersion", *Physikalische Zeitschrift Der Sowjetunion*, vol. 10, 1936.

[25] R. C. Millikan, and D. R. White, "Systematics of Vibrational Relaxation", *Journal of Chemical Physics*, vol. 39, pp. 3209–3213, 1963.

[26] C. Park, *Nonequilibrium Hypersonic Aerothermodynamics*, Wiley International, New York, NY, USA, 1990.

[27] D. A. Andrienko, "Non-Equilibrium Models for High Temperature Gas Flows", Ph.D. Thesis, Moscow Institute of Physics and Technology, Dolgoprudny, Russia, 2014.

[28] O. Knab, H. H. Frühauf, and E. W. Messerschmid, "Theory and Validation of the Physically Consistent Coupled Vibration - Chemistry Vibration Model", *Journal of Thermophysics and Heat Transfer*, vol. 9, pp. 219–226, April 1995.

[29] O. Knab, H. H. Frühauf, and S. Jonas, "Multiple Temperature Descriptions of Reaction Rate Constants with Regard to Consistent Chemical-Vibrational Coupling", *In Proceedings of the 27th Thermophysics Conference, AIAA 1992*, Nashville, TN, USA, July 6–8, 1992.

[30] L. Scalabrin, "Numerical Simulation of Weakly Ionized Hypersonic Flow over Reentry Capsules", Ph.D. dissertation, The University of Michigan, Ann Arbor, MI, USA, 2007.

[31] P. V. Marrone, and C. E. Treanor, "Chemical relaxation with preferential dissociation from excited vibrational levels", *The Physics of Fluids*, vol. 6, pp. 1215–1221, 1963.

[32] G. A. Bird, "*The DSMC Method*", 2nd ed., Create Space Independent Publishing Platform, Sydney, Australia, 2013.

[33] "*CHEMKIN*", en.wikipedia.org. [Online].Available: https://en.wikipedia.org/wiki/CHEMKIN. [Accessed: Sept. 20, 2020]

[34] S. J. Gordon, B. J. McBride, and M. J. Zehe, "NASA Glenn Coefficients for Calculating Thermodynamic Properties of Individual Species", Glenn Research Center, Cleveland, Ohio, Tech. Rep. NASA/TP-2002-211556, 2002.

[35] I. D. Boyd, and E. Josyula, "State resolved vibrational relaxation modeling for strongly nonequilibrium flows", *Physics of Fluids*, vol. 23, 2011.

[36] C. Park, "Assessment of two-temperature kinetic model for dissociating and weakly ionizing nitrogen," *Journal of Thermophysics and Heat Transfer*, vol. 2, July 1986.

[37] C. Park, "Assessment of two-temperature kinetic model for ıonizing air," *4th Thermophysics and Heat Transfer Conference*, Boston, MA, U.S.A, June 2-4, 1986.

[38] J. C. Maxwell, "On stresses in rarefied gases arising from inequalities of temperature", *Philosophical Transactions of the Royal Society of London*, vol. 170, pp. 231–256, 1879.

[39] M. Von Smoluchowski, "Uber wärmeleitung in verdünnten Gasen", *Annalen der Physik*, vol. 300, pp. 101–130, 1898.

[40] M. MacLean, M. Holden, and A. Dufrene, "Comparison Between CFD and Measurements for Real-Gas Effects on Laminar Shock Wave Boundary Layer Interaction, I", *AIAA Aviation 2014*, AIAA, Reston, VA, 2014.

[41] N. Kianvashrad, and D. Knight, "The effect of thermochemistry on prediction of aerothermodynamic loading over a double cone in a laminar hypersonic flow," *2018 AIAA Aerospace Sciences Meeting, AIAA 2018*, Kissimmee, Florida, January 8-12, 2018.

[42] C. Park, "On convergence of computation of chemically reacting flow," *23rd Aerospace Sciences Meeting, AIAA 1985, Reno, NV, USA*, January 14-17, 1985.

VITAE

Davut VATANSEVER received his B.Sc. degree in Mechanical Engineering from Faculty of Mechanical Engineering, Yildiz Technical University, Turkey in 2016. He received his M.Sc. degree in Aeronautical and Astronautical Engineering from Istanbul Technical University, Turkey in 2020. He is currently working at Istanbul Technical University as Research Assistant.

Bayram ÇELİK received his B.Sc. degree in Astronautical Engineering from Faculty of Aeronautical and Astronautical Engineering, Istanbul Technical University, Turkey in 1993. He received his M.Sc. and PHD degree in Aeronautical and Astronautical Engineering from Istanbul Technical University, Turkey in 1997 and 2006, respectively. He is currently working at Istanbul Technical University as Associate Professor.